sciendo Journal of Electrical Engineering, Vol. 76, No. 1, 2025, pp. 58-71

Voltage dips and swells detection by sliding fast Fourier transform: Possibilities for application in modern distribution networks

Mladen Banjanin[1], Miloš Milovanović[2], Jordan Radosavljević[2]

This paper deals with applying the sliding Fast Fourier Transform analysis to detect voltage dips and swells in modern distribution networks. Significant odd and even voltage harmonics appear during voltage dips and swells, and they can be used to detect these events. Since the voltage waveshape during the dips and swells have the same harmonic content, the separation of these events can be done by calculating the angles of the voltage harmonics at the moment of the event. In the case of voltage swells phase angles of the 1st and the higher order harmonics have the same polarity, while in the case of voltage dips phase angles of the 1st and of the higher order harmonics have the opposite polarity. The presented approach is verified by analyzing mathematical signals and signals measured in real distribution networks with renewable sources. The limitation of the analyzed method is that the amplitude of voltage variation during the dip or swell in a real distribution network cannot be reliably associated with the calculated values of voltage harmonics. This limitation can be overcome by considering the value of 1st voltage harmonic, or RMS voltage value calculated for one cycle or half cycle of the voltage wave.

Keywords: distribution network, harmonics, power quality, renewable sources, sliding Fast Fourier Transform, voltage dip, voltage swell

1 Introduction

Analysis of the electric power quality (PQ) in the low voltage and medium voltage electric power distribution networks (DNs) is becoming more and more important because of many nonlinear loads and nonlinear sources of the electric power connected to the DNs [1-3]. These types of loads and sources have a negative impact on the PQ in DNs but also suffer the consequences of the poor PQ [3,4]. Voltage quality in the DNs is mainly analyzed in accordance with EN 50160 [5]. Both voltage and current quality can be analyzed in accordance with standards IEEE 1159-2009 [6] or IEEE 519-2022 [7]. Voltage dips and swells are very important parameters of the PQ since they significantly impact the operation of different types of loads and sources. According to the mentioned standards, including the standard IEC 61000-4-30:2021 [8], a voltage dip, also known as voltage sag, is defined as a decrease in the root mean square (RMS) voltage from 10% to 90% of the rated voltage value for the duration of the half cycle (10 ms for 50 Hz voltage) to 1 min. The voltage swell is also defined in the same standards, as an increase in the RMS voltage above 110% of the rated voltage value for the duration of the half cycle to 1 min. Each voltage event, like dip, swell, or interruption, is categorized by locating them in the magnitude-duration plane, following an assessment of the event's magnitude and duration. The general approach is that each event is categorized into one of the categories and cannot simultaneously belong to several categories.

Voltage dips and swells are mainly caused by short circuit faults in the electric transmission or distribution systems, back-flashovers on the overhead lines caused by lightning strikes, operation of large electric drives and loads, load rejection, problems with voltage regulation, etc [9]. These voltage events can cause problems in the operation of sensitive electronic equipment, computers, digitally controlled industrial drives, etc. Because of that, there are different standards and technical documents that define immunity curves for such sensitive equipment, like CBEMA/ICIT curves, SEMI F47, and IEC 61000-4-11/34 [10]. Various solutions were proposed to ensure uninterrupted operation of equipment during the voltage dips, such as installation of uninterruptible power supply (UPS) or other types of energy storage devices, application of series active power filters (APFs), and dynamic voltage restorers (DVRs), implementation of series and shunt controllers based on voltage-source converters (VSCs), etc [11]. The devices and techniques mentioned need fast voltage dips/swells detection methods, mostly up to 5 ms or 10 ms [11].

Traditionally, voltage dips and swells are detected based on the estimation of the RMS voltage value. This method is efficient and reliable, but at the same time, it is time-consuming since it requires 1 or 2 cycles of voltage to ensure proper event detection (i.e., from 20 ms up to 40 ms for the 50 Hz voltage) [11]. Because of that many specific voltage dip detection methods are introduced, such as Symmetrical Components Algo-

[1] Faculty of Electrical Engineering, University of East Sarajevo, East Sarajevo, 71123, Bosnia and Herzegovina
[2] Faculty of Technical Sciences, University of Priština in Kosovska Mitrovica, Kosovska Mitrovica, 38220, Serbia
mladen.banjanin@etf.ues.rs.ba, milos.milovanovic@pr.ac.rs, jordan.radosavljevic@pr.ac.rs

https://doi.org/10.2478/jee-2025-0006, Print (till 2015) ISSN 1335-3632, On-line ISSN 1339-309X

rithm (SCA) [12], three-phase voltage ellipse parameters method [13], wavelet transform-based voltage dip/swell detection algorithms [14, 15], multi-dimension characterization method [16], method based on the Independent Component Analysis (ICA) [17], Kalman filter [18], Selective Harmonic Extraction (SHE) algorithm [19], Second Order Generalized Integrator (SOGI), time-delay transform methods [20], etc. Methodology for smart and fast detection of voltage dips based on the adjusted Recurrent Neural Network is presented in [11], enabling the detection of voltage dips in less than 1 ms. In addition, the method of voltage dip detection based on the harmonic content of the signals is analyzed in [11,21-24]. This method is based on the sliding Fast Fourier Transform (SFFT) of a voltage signal and detecting specific harmonics that appear during a voltage dip. The SFFT algorithm is applied in [21] for the detection of voltage dips in the large database of measured voltage waveshapes. The calculation window was not of fixed size and by widening the window it was possible to analyze large datasets and to detect voltage and current disturbances. In [11, 22-24], authors investigated different values of voltage harmonics or values of their combinations which can be used to indicate the appearance of the voltage dips. Based on many combinations, authors finally suggest the set of the 2nd, 3rd, 5th, and 7th voltage harmonics as optimum for voltage dip detection [22], and in [11] named it the Harmonic Footprint (HFP).

To the best of the authors' knowledge, the methodology based on the SFFT and HFP of the voltage signals has been applied exclusively to detect voltage dips. This paper presents the method based on the SFFT applicable to detect both voltage dips and swells. That is achieved by analyzing not only the amplitude of the voltage harmonics during the events but also their phase angle. It is presented that in the case of voltage swells phase angles of the higher-order voltage harmonics have the same polarity as the phase angle of the 1st voltage harmonic, while in the case of voltage dips phase angles of the higher-order voltage harmonics have the opposite polarity compared to the phase angle of the 1st voltage harmonic. The applicability of the proposed method is tested on the mathematical signals and signals measured in real DNs with photovoltaic (PV) power plants and large nonlinear loads (regulated electric drives). The method is fully efficient in the case of mathematical signals. In the case of signals measured in real DNs, the method is fully efficient in detecting voltage dips and swells but has limited accuracy in the correlation of calculated values of HFPs and the values of voltage variations. This is caused by the significant impact of harmonics generated by nonlinear sources and loads on the calculated HFP during the dips and swells.

2 Mathematical and measured signals used to test the suggested method of voltage dips and swell detection

The possibility of SFFT analysis application for voltage dips and swells detection is tested by using two types of signals, mathematical signals and signals measured in real DNs.

Mathematical signals of voltage dips and swells are generated by using Eqn. (1). The duration of the dips and swells is limited to 40 ms to make figures more readable and to make it easier to see changes in the values of the harmonics and their phase angles. This has not had any impact on the presented results and applied method since in the case of sinusoidal signals higher-order harmonics appear only in the transient periods, during the appearance and disappearance of the dips and swells.

$$u(t)=\begin{cases}\sqrt{2}U_{nPH}\sin(2\pi ft+\varphi), & t\le 40\text{ ms}\wedge t\ge 80\text{ ms}\\ \sqrt{2}k_1U_{nPH}\sin(2\pi ft+\varphi), & 40\text{ ms}<t<80\text{ ms}\end{cases} \quad (1)$$

where U_{nPH} is the rated RMS phase voltage value, 230 V, f is the rated frequency, 50 Hz, t is the time (s), k_1 is the amplitude coefficient, and φ is the voltage phase angle (rad).

Besides these mathematical signals, voltage waveshapes measured in real DNs are also used. Measurements of voltage events are made by using the three-phase power quality analyzer of class A [25]. In total, 10 different measuring points are considered. Measurements are conducted in seven-day periods and the total duration of the measurements was 70 days. About 137 voltage events (dips and swells) were detected. The sampling frequency was 7 kHz and it was defined by measuring instrument. The same sampling frequency is applied for mathematically generated signals defined by Eqn. (1). Conducted experimental measurements can be grouped into four scenarios:

Scenario I: Rural DNs with several PV power plants connected to the 10 kV overhead lines. Measurements are conducted in the points of common coupling (PCC) of four PV power plants with rated power between 150 kW and 235 kW. The measuring instrument is connected at the 0.4 kV voltage level of the 10/0.4 kV/kV pole-mounted transformer.

Scenario II: Rural DN with a small hydropower plant (SH power plant) supplying large nonlinear loads (regulated electric drives in the nearby quarry). In the registration period output power of the SH power plant was up to 800 kW. The measuring instrument was connected at the 10 kV side of the power transformer and measured voltage and current signals are used from the instrument transformers.

Scenario III: Urban DNs with several PV power plants connected to the 10 kV overhead lines. Measurements are conducted in the PCC of four PV power plants with rated power between 16 kW and 150 kW. The measuring instrument is connected to the 0.4 kV voltage level of the 10/0.4 kV/kV power transformer.

Scenario IV: Internal DN of the large PV power plant (50 MW) connected to the 220 kV overhead transmission lines. Measurements are conducted at the 0.8 kV voltage level of the power transformer 20/0.8 kV/kV, with an installed power of 1250 kVA.

The coupling of power transformers was Dyn (delta configuration ("D") at the 10 kV and 20 kV voltage levels, and wye configuration with grounded neutral ("yn") at the 0.4 kV and 0.8 kV voltage levels).

3 Detection of voltage dips and swells by using the SFFT

An example of the PV power plant trip out due to a voltage dip is presented in Fig. 1. In this case the voltage dip appears in two phases. Shortly after the trip out of the PV power plant the voltage dip disappears, and the voltage regains nominal values. So, the voltage dips and swells can produce malfunction of the equipment in the DNs, and these events need to be properly and fast detected to prevent such scenarios.

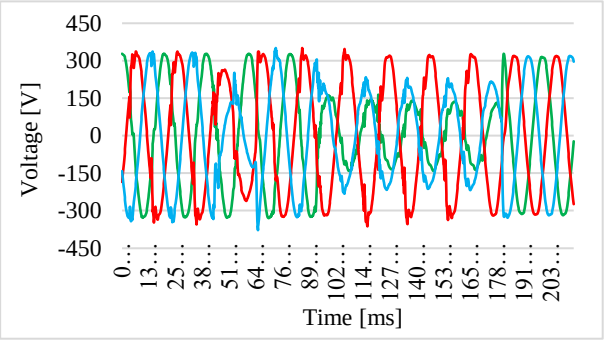

(a)

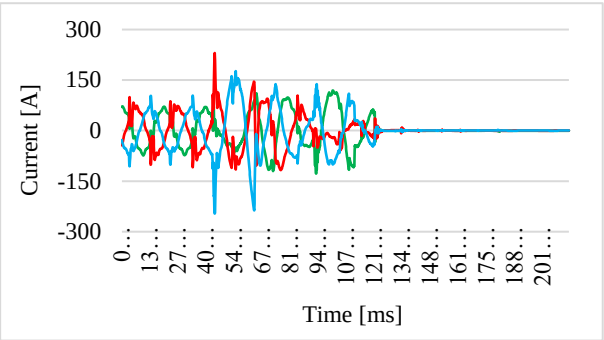

(b)

Fig. 1. Trip out of the PV power plant due to the voltage dip: (a) three-phase voltages, (b) three-phase currents

The SFFT is in calculations applied as follows:

- Fast Fourier Transform (FFT) and SFFT analyses are done by using the script file implemented in MATLAB software [26]. MATLAB's function "fft" is applied to one cycle window of the power frequency voltage (20 ms), and in that way, standard FFT analysis for the one period of voltage wave is done (for example T1-T11 in Fig. 2).
- SFFT analysis is done based on the standard FFT analysis. RMS voltage values and voltage harmonics are continually calculated, and results are updated with each new sample taken. This is illustrated in Fig. 2. In the first step standard FFT analysis is done for one period of the signal marked as T1-T11. After that the calculation window is updated with one new sample (ΔT is the sampling period) and FFT analysis is done for the new period of the signal marked in Fig. 2 as T2-T22. The procedure is repeated for all samples of the signal.

The sampling frequency in all measurements was 7 kHz, and the same sampling frequency was applied in all algorithms, both for mathematical and measured signals.

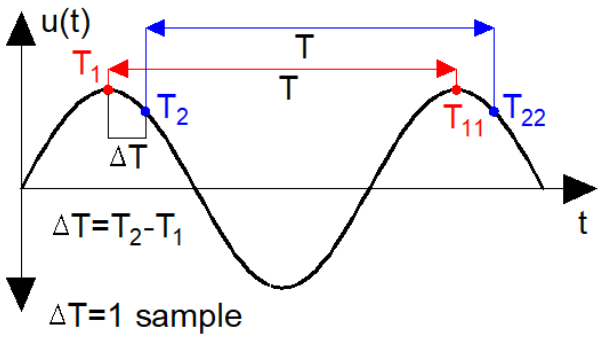

Fig. 2. Explanation of the SFFT analysis applied in calculations

3.1 Analysis of the mathematical signals

In Table 1 are given values of individual voltage harmonics and of the HFP calculated during the voltage dips and swells. The HFP is calculated for the following combinations of voltage harmonics: $2^{nd}+3^{rd}$, $2^{nd}+3^{rd}+4^{th}$, $2^{nd}+3^{rd}+4^{th}+6^{th}$, $2^{nd}+3^{rd}+4^{th}+5^{th}+6^{th}+7^{th}$ and $2^{nd}+3^{rd}+5^{th}+7^{th}$. Values of all harmonics are calculated relative to the amplitude of the rated phase voltage. Calculations are performed with mathematical signals generated by using Eqn. (1). According to Tab. 1, the values of voltage harmonics and HFP (exception is 3^{rd} harmonic) are more pronounced if the voltage amplitude variation is larger, as well as if voltage dip or swell appears in the moment when the voltage value is higher. In the case of small voltage variation values of some harmonics can be low, however, HFP has larger values and can be a better

indicator of the voltage event. That is very important in the case of real measured signals from the DNs because of the voltage waveshape distortion due to harmonics and due to signal noise. The same harmonic values are calculated both for voltage dips and swells if the voltage variation compared to the rated voltage value is the same (if harmonics are calculated relative to the 1st harmonic this is not satisfied). This means that a decrease or increase of the voltage for some value ΔU led to the same values of voltage harmonics and HFP. Because of that, the same methodology can be applied for the detection of both voltage dips and swells. The values of test voltages equal to 206 V and 254 V are selected because international standards [5-8] define that the voltage dip is the voltage event when the voltage amplitude reduces below 0.9 of the rated voltage, while the voltage swell is the event when the voltage amplitude increases above 1.1 of the rated voltage.

Table 1. Voltage harmonics during the voltage dips and swells in the case of mathematical signals generated by using Eqn. (1)

HFP	$k_1 \cdot U_{nPH}$ (206 V or 254 V)			$k_1 \cdot U_{nPH}$ (100 V or 360 V)		
	$\varphi=0$ or π	$\varphi=\pi/4$ or $3\pi/4$	$\varphi=\pi/2$ or $3\pi/2$	$\varphi=0$ or π	$\varphi=\pi/4$ or $3\pi/4$	$\varphi=\pi/2$ or $3\pi/2$
2nd	2.9%	3.8%	4.4%	15.6%	20.3%	24.0%
3rd	1.7%	2.1%	1.9%	9.0%	11.4%	10.5%
4th	1.1%	1.5%	1.8%	5.7%	8.4%	9.6%
5th	0.7%	1.2%	1.3%	3.9%	6.5%	6.9%
6th	0.7%	1.0%	1.1%	3.5%	5.3%	6.2%
7th	0.6%	0.8%	0.9%	3.0%	4.4%	5.0%
2nd+3rd	4.3%	5.3%	5.4%	23.4%	28.5%	29.4%
2nd+3rd+4th	5.1%	6.2%	6.7%	27.6%	33.7%	36.2%
2nd+3rd+4th+6th	5.7%	6.5%	7.6%	31.0%	35.4%	41.2%
2nd+3rd+4th+5th+6th+7th	6.8%	8.1%	9.1%	37.0%	43.7%	49.5%
2nd+3rd+5th+7th	5.4%	7.1%	7.6%	29.4%	38.4%	40.9%

As presented in Tab. 1, the same values of individual voltage harmonics and HFP are calculated if the voltage variation compared to the rated voltage value is the same, consequently, it is not possible to distinguish voltage swells and dips by calculating only values of harmonics. By introducing the harmonic phase angle polarity in the moment of voltage event it is possible to distinguish voltage dips and swells, as presented in Figs. 3 to 6., in the following manner:

- In the case of voltage dips the phase angles of the higher-order voltage harmonics have opposite polarity compared to the 1st voltage harmonic because higher-order voltage harmonics must be subtracted from the 1st voltage harmonic.
- In the case of voltage swells the phase angles of the higher voltage harmonics have the same polarity as the 1st voltage harmonic because higher-order voltage harmonics must be added to the 1st voltage harmonic.

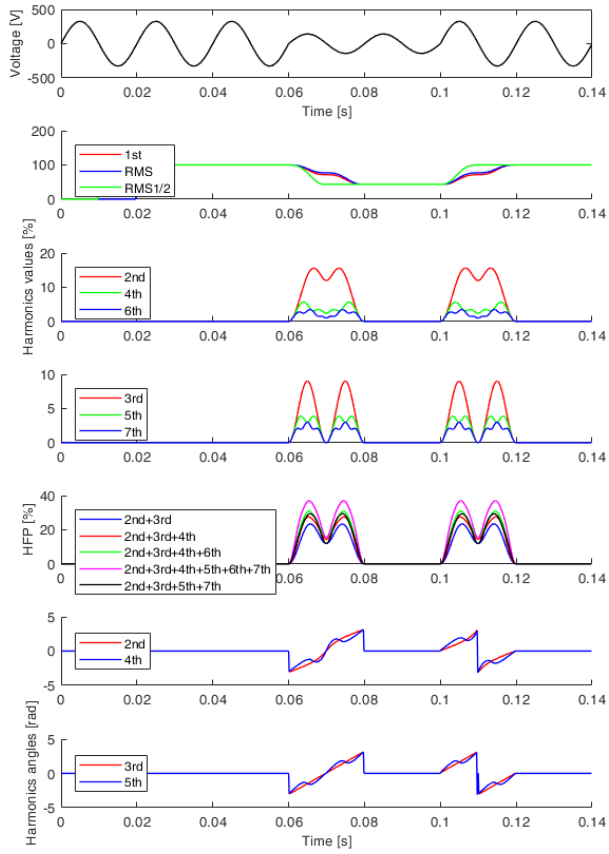

(a)

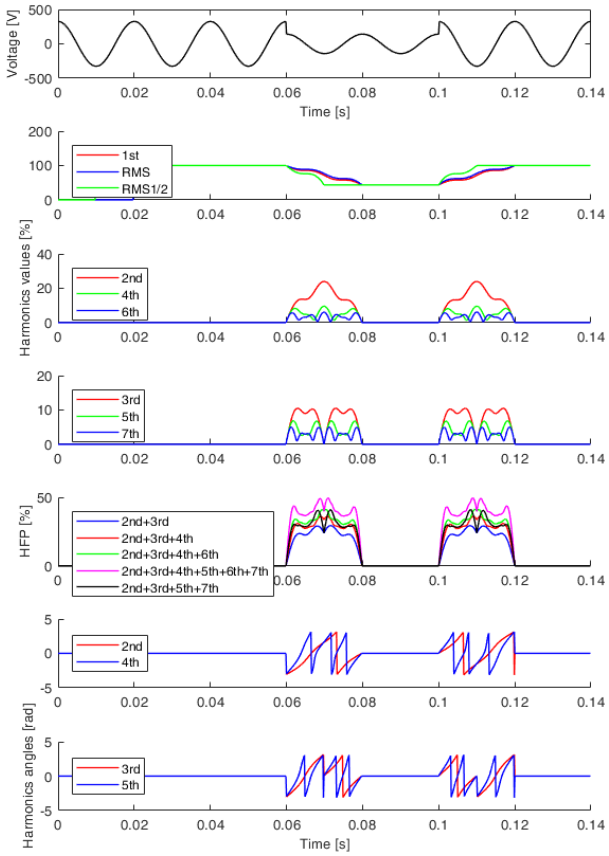

(b)

Fig. 3. Harmonic content of the signal during the voltage dip in positive half-cycle of the power frequency voltage (1), $k_1 \cdot U_{nPH}$=100 V: (a) φ=0, (b) $\varphi=\pi/2$

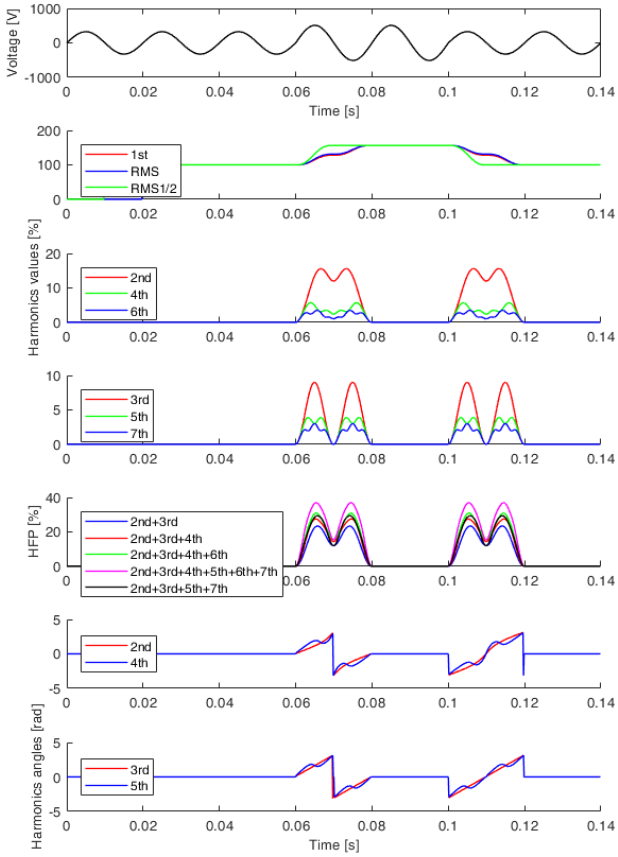

(a)

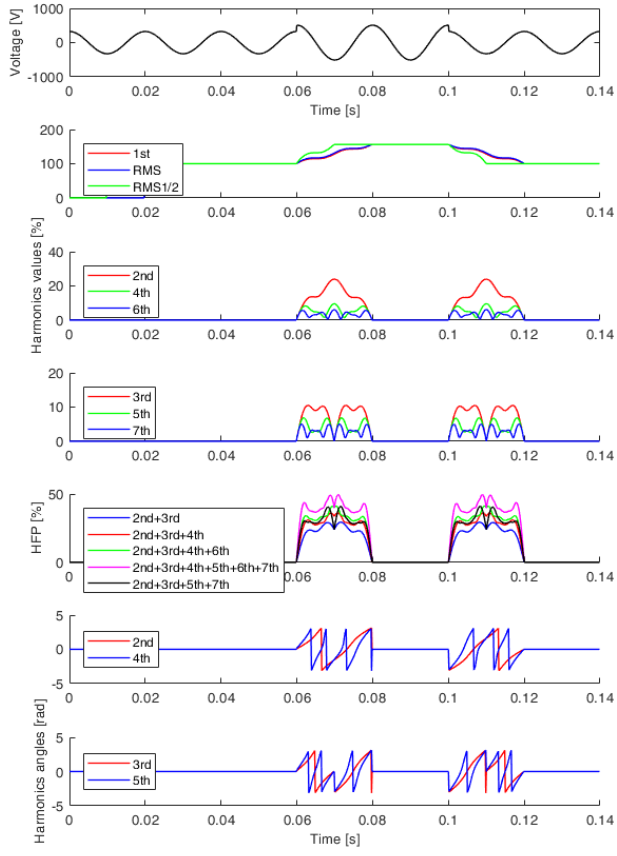

(b)

Fig. 4. Harmonic content of the signal during the voltage swell in positive half-cycle of the power frequency voltage (1), $k_1 \cdot U_{nPH}$=360 V: (a) φ=0, (b) $\varphi=\pi/2$

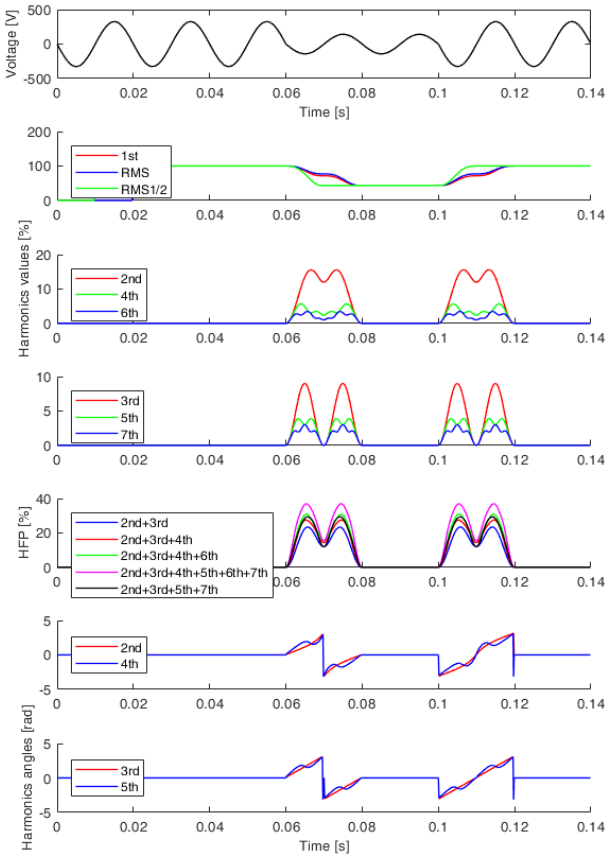

(a)

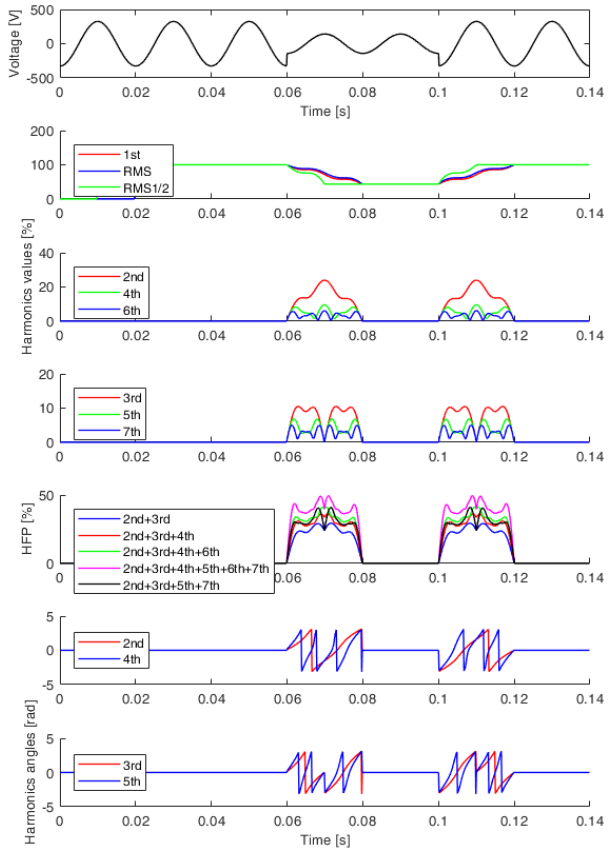

(b)

Fig. 5. Harmonic content of the signal during the voltage dip in negative half-cycle of the power frequency voltage (1), $k_1 \cdot U_{nPH}$=100 V: (a) $\varphi=\pi$, (b) $\varphi=3\pi/2$

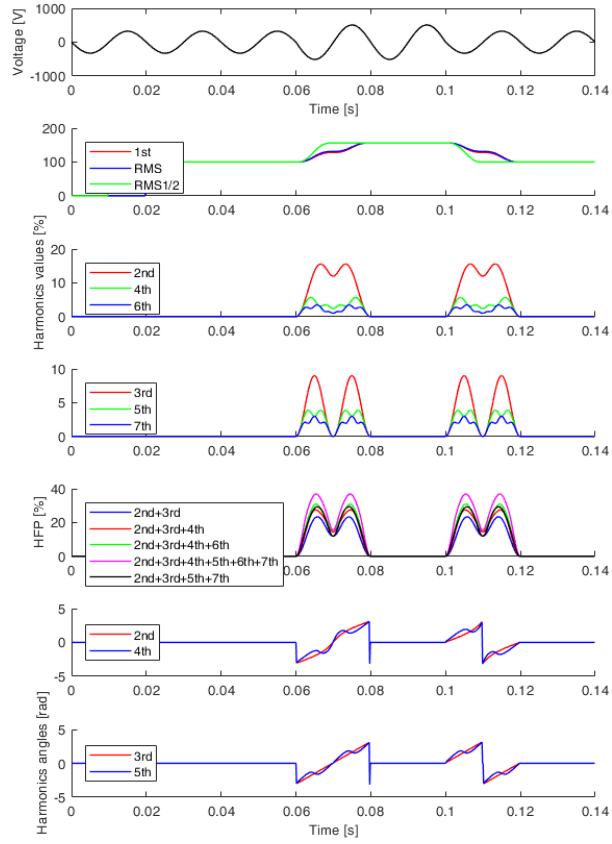

(a)

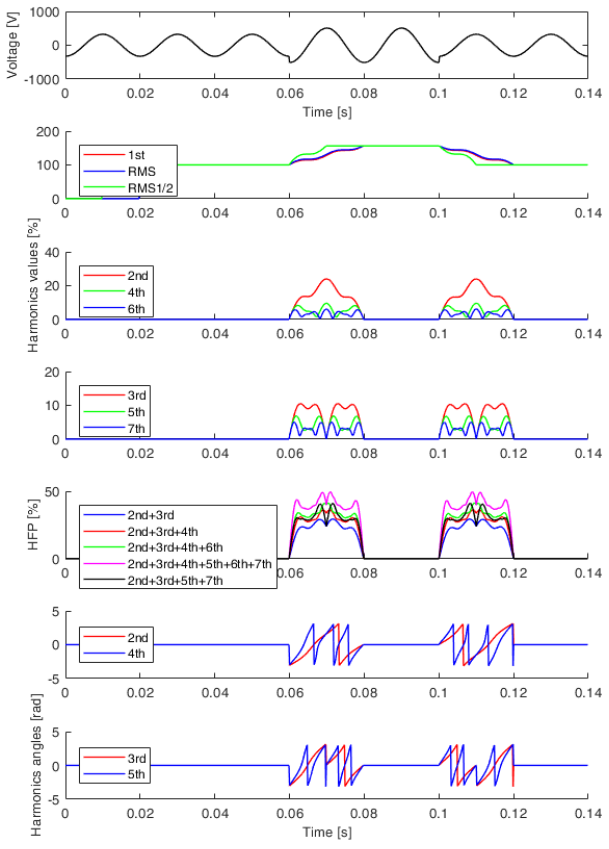

(b)

Fig. 6. Harmonic content of the signal during the voltage swell in negative half-cycle of the power frequency voltage (1), $k_1 \cdot U_{nPH}$=360 V: (a) $\varphi=\pi$, (b) $\varphi=3\pi/2$

In Fig. 3, the harmonic content of the phase voltage is calculated under the conditions of a voltage dip in the positive half cycle of the voltage wave, specifically showing the voltage RMS value decrease from 230 V to 100 V. In Fig. 3a the harmonic content of the signal is illustrated for the phase angle $\varphi = 0$ in Eqn. (1), while in Fig. 3b it is illustrated for the phase angle $\varphi = \pi/2$ in Eqn. (1). In the case when the voltage RMS value starts to decrease the phase angles of the 2nd, 3rd, 4th, and 5th voltage harmonics become negative because the phase angle of the 1st voltage harmonic is positive. In the case when the voltage RMS value starts to increase to the rated value, the phase angles of the same voltage harmonics become positive because the phase angle of the 1st voltage harmonic is positive. The same conclusions state for the voltage swell which appears in the positive half cycle of the voltage wave, as can be seen in Fig. 4. In Fig. 4, the harmonic content of the phase voltage is illustrated specifically showing the voltage RMS value increase from 230 V to 360 V. In Fig. 4a, the harmonic content is depicted for the phase angle $\varphi = 0$ in Eqn. (1), whereas in Fig. 4b, it is illustrated for the phase angle $\varphi = \pi/2$ in Eqn. (1). Calculations are repeated for the case when the voltage dip and swell appear in the negative half-cycle of the power frequency voltage. Estimated results are presented in Fig. 5 and Fig. 6. Voltage dip which appears in the negative half-cycle of the power frequency voltage causes voltage harmonics to have a positive phase angle, while voltage swell which appears in the negative half-cycle of the power frequency voltage causes that voltage harmonics have negative phase angle.

In Figs. 3 to 6, the RMS and 1st harmonic voltage values agree very well, while the RMS1/2 voltage value (RMS voltage value calculated for the 10 ms period) converged much faster (two times) compared to them and can be used for faster detection of voltage dips or swells. Also, voltage harmonics and HFP appear only during the transient periods of voltage dip or swell, in two periods equal to 20 ms each.

3.2 Analysis of the signals measured in real DNs

Verification of the method presented in the previous section and based on the mathematical signals is done by analyzing signals measured in real DNs. The calculated results are presented in Figs. 7 to 10. Abbreviations "EH" and "OH" in the figures indicate the even and odd voltage harmonics, respectively.

Table 2 summarizes calculated values of voltage variation and corresponding values of individual harmonics and HFP for signals presented in Figs. 7 and 8. Values of all harmonics are calculated relative to the amplitude of the rated phase voltage. Signals presented in Fig. 7c and in Fig. 7d have almost the same voltage variation (about 22%). In contrast, calculated values of harmonics and HFP are significantly different (about 3.5 times). Also, the signal presented in Fig. 7c has more than two times lower voltage variation in comparison to the signal presented in Fig. 7b but has larger values of almost all harmonics and HFP. This is caused by the significant distortion of the voltage waveshape presented in Fig. 7c. This limitation of the proposed method is analyzed in more detail in section 3.3, while in this section it is proved that simultaneous analysis of the voltage harmonics and their phase angles values can be used as a reliable indicator of the voltage dips and swells in real DNs.

Table 2. Values of voltage variation and corresponding values of harmonics and HFP during the voltage dips and swells in the case of real signals measured in DNs

Voltage variation (%)	16.6	49.7	22.1	22.7	15.9
HFP	Calculated values (%) in Figure				
	7a	7b	7c	7d	8
2nd	6.5	20.7	26.5	6.9	9.8
3rd	4.2	13.2	15.4	4.7	9.2
4th	3.4	7.5	12.0	3.3	5.1
5th	3.6	11.9	10.2	5.3	3.6
6th	3.6	12.9	10.1	3.0	3.6
7th	3.8	9.6	7.1	1.9	4.0
2nd+3rd	9.1	28.8	35.4	10.4	16.8
2nd+3rd+4th	11.0	33.6	44.0	13.1	19.3
2nd+3rd+4th+6th	14.2	41.2	52.5	14.6	21.7
2nd+3rd+4th+ +5th+6th+7th	19.4	53.4	62.1	17.8	24.4
2nd+3rd+5th+7th	15.1	45.1	50.2	15.2	19.6

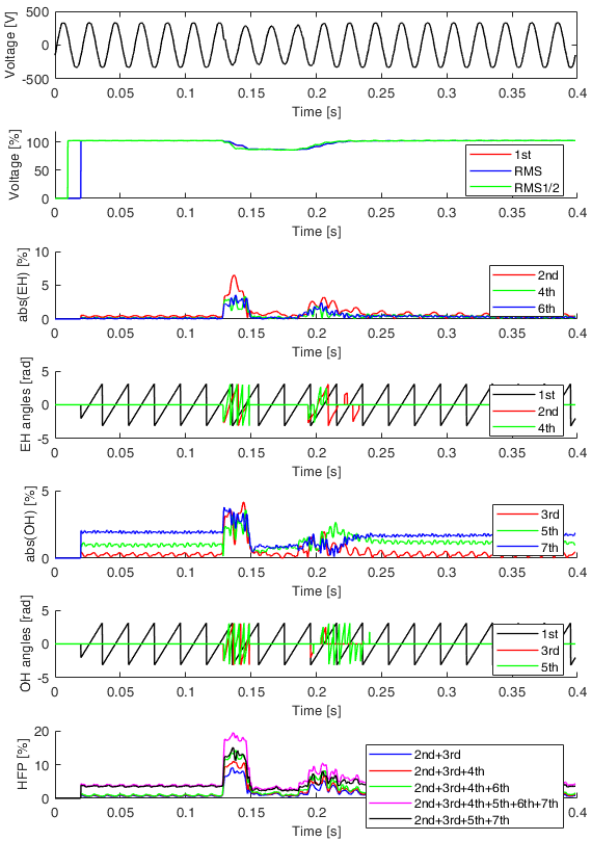

(a)

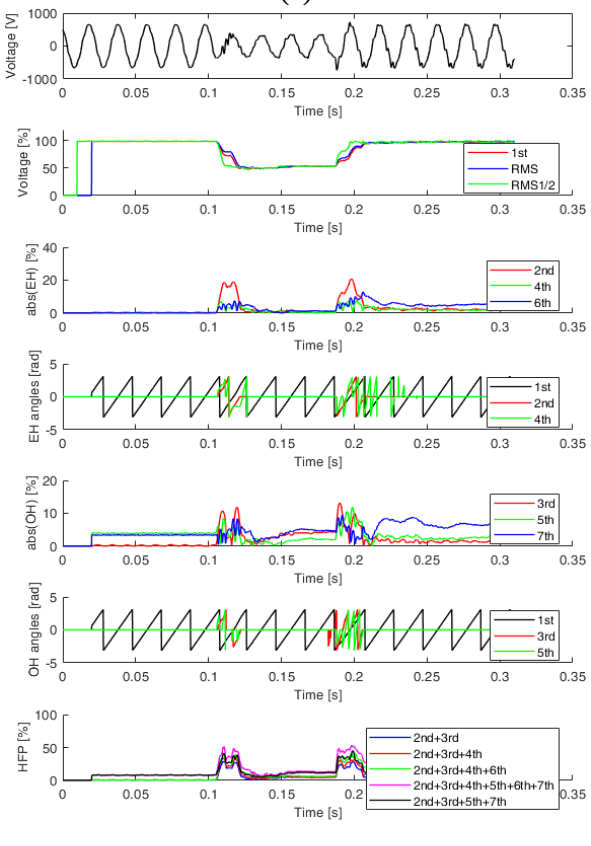

(b)

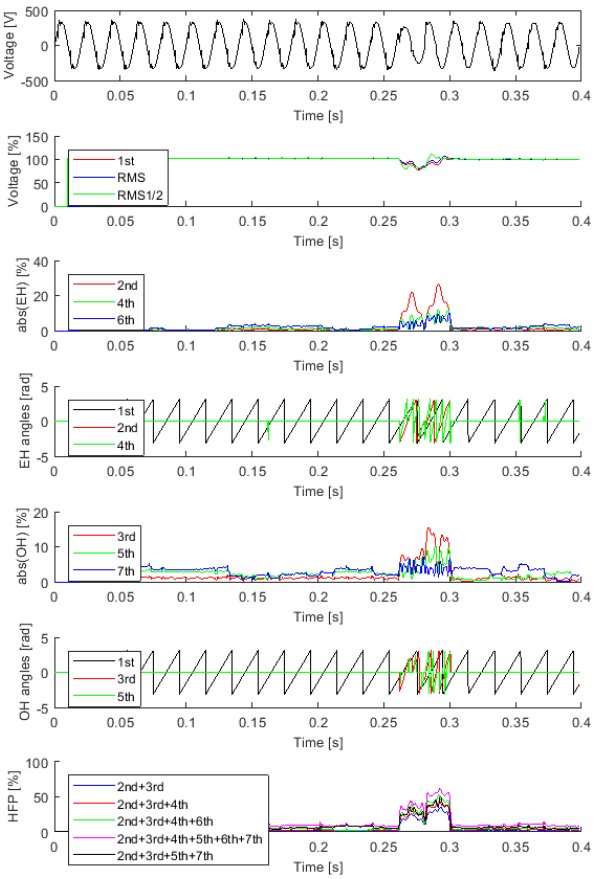

(c)

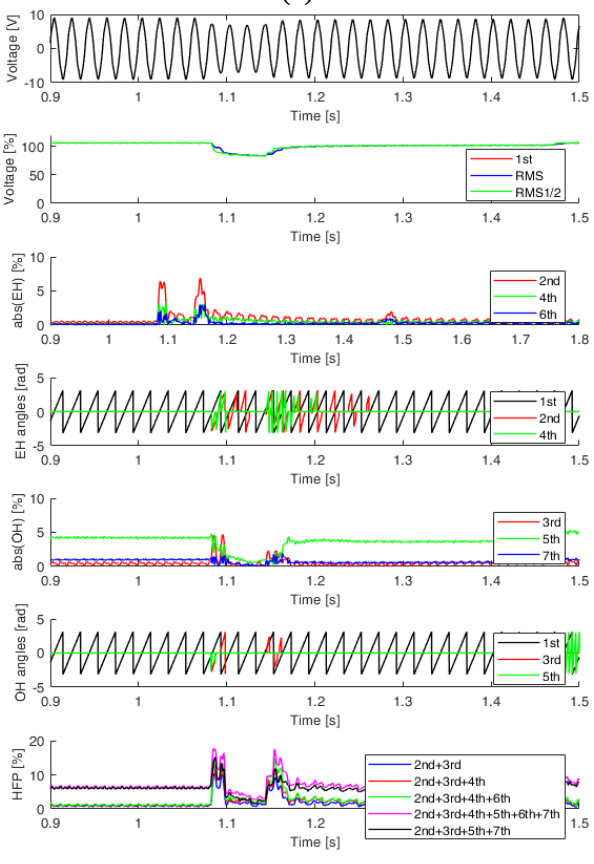

(d)

Fig. 7. The SFFT analysis application to the voltage dip detection for the signals measured at the PCC: (a), (b), (c) of the PV power plants, (d) of the SH power plant

In Fig. 7, examples of voltage dips detection are presented. During all dip events significant even and add voltage harmonics are calculated, and in all cases phase angles of the higher order voltage harmonics in the moment of the voltage dip have the opposite polarity compared to the 1st voltage harmonic. The algorithm is sensitive in the DNs with different rated voltages equal to 0.4 kV, 0.8 kV, and 10 kV. The suggested method is sensitive for signals whose waveshape is significantly distorted with harmonics, as in Fig. 7b and Fig. 7c. It also can be observed that RMS, RMS1/2, and 1st harmonic voltage values agree very well, and RMS1/2 voltage value converged about two times faster compared to RMS and 1st harmonic values.

Figure 8 illustrates the application of the proposed method on the detection of the voltage swell for the signal measured at the 0.4 kV voltage level in the PCC of the PV power plant. In the moment of voltage swell 1st and higher-order harmonics have the same polarity proving that the suggested method of voltage swell detection is efficient for signals measured in real DNs.

Figure 9 presents the application of the SFFT analysis on the voltage signals measured at the PCC of the PV power plants during the voltage interruptions. In Fig. 9a the voltage dip and voltage interruption are presented, in Fig. 9b voltage swell, dip, and interruption are presented, while in Fig. 9c voltage dip, swell, and interruption are presented. It can be observed that the voltage RMS1/2 value better corresponds to the real RMS signal value in comparison to the 1st voltage harmonic value, especially in Fig. 9b and Fig. 9c where voltage variations are more pronounced. It also can be observed that the calculation of the voltage harmonics values and their phase angles in the moment of the dips and swells can be reliably used to detect these voltage events.

In Fig. 10, the application of the SFFT analysis on the voltage signals measured at the PCC of the PV power plants is presented during the voltage switching on. Fig. 10a presents a case when switching on appears in the positive half cycle of the voltage wave, while Fig. 10b presents a case when switching on appears in the negative half cycle of the voltage wave. The polarities of the phase angles of higher-order voltage harmonics in the moment of voltage switching are the same as the phase angle of the 1st voltage harmonic. It also can be observed that the RMS1/2 value converges faster to the steady state value compared to the RMS and 1st harmonic values.

Based on the presented results it can be concluded that calculation of the voltage harmonics values and their phase angles polarities can be used for reliable detection of voltage swells and dips both in the case of mathematical signals and in the case of the signals measured in real DNs, despite significant harmonic distortion of the voltage waveshape due to nonlinear sources (PV power plants) and loads (regulated electric drives) of the electric power.

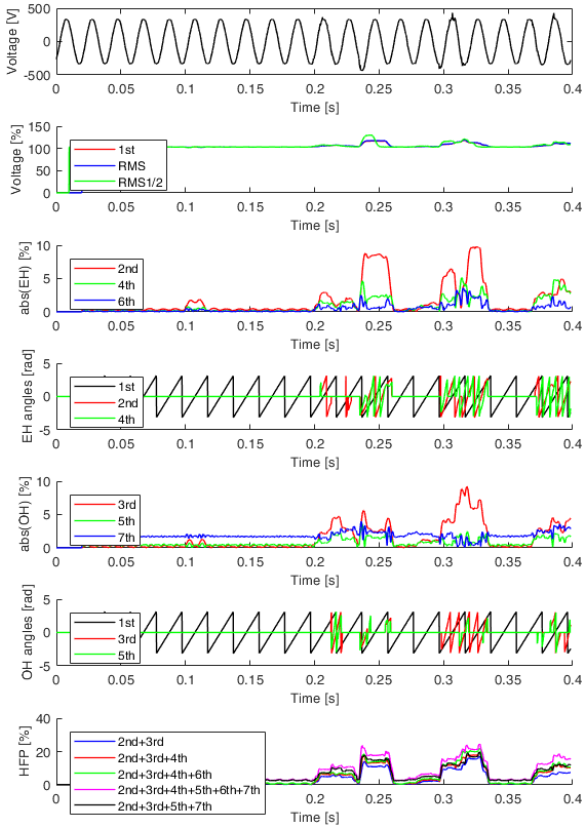

Fig. 8. The SFFT analysis application to the voltage swell detection for the signal measured at the PCC of the PV power plant

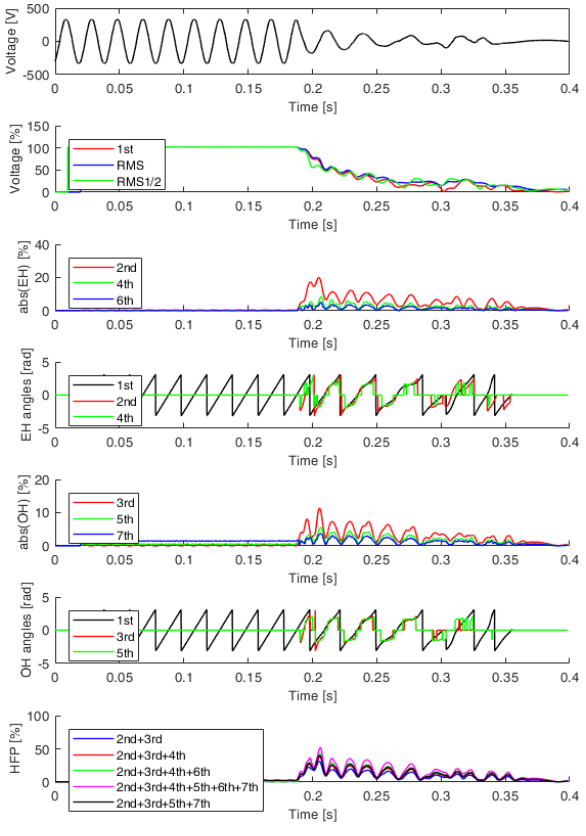

(a)

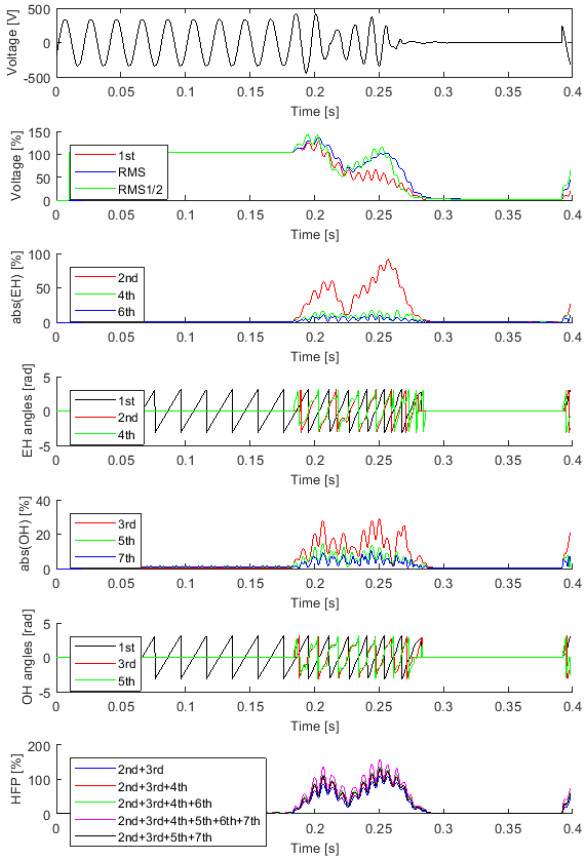

(b)

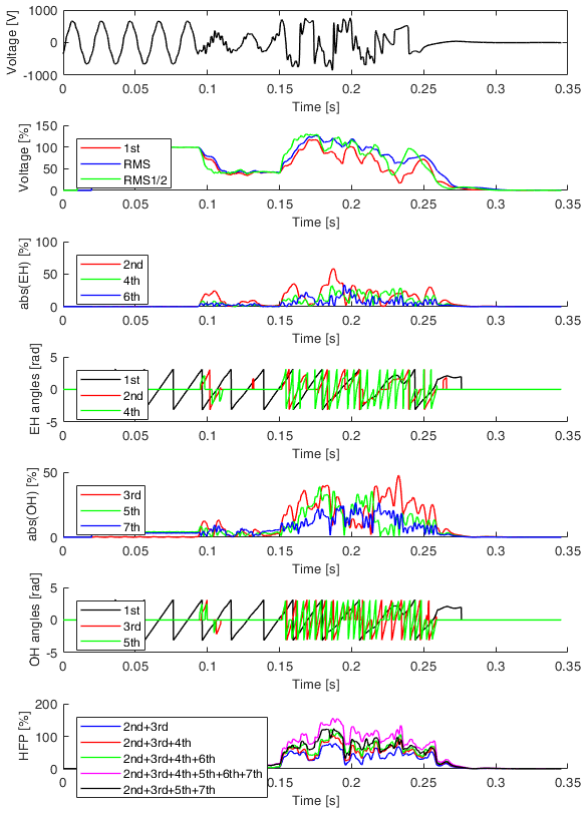

(c)

Fig. 9. The SFFT analysis application on the voltage signals measured at the PCC of the PV power plants: (a) voltage dip and interruption, (b) voltage swell, dip, and interruption, (c) voltage dip, swell, and interruption

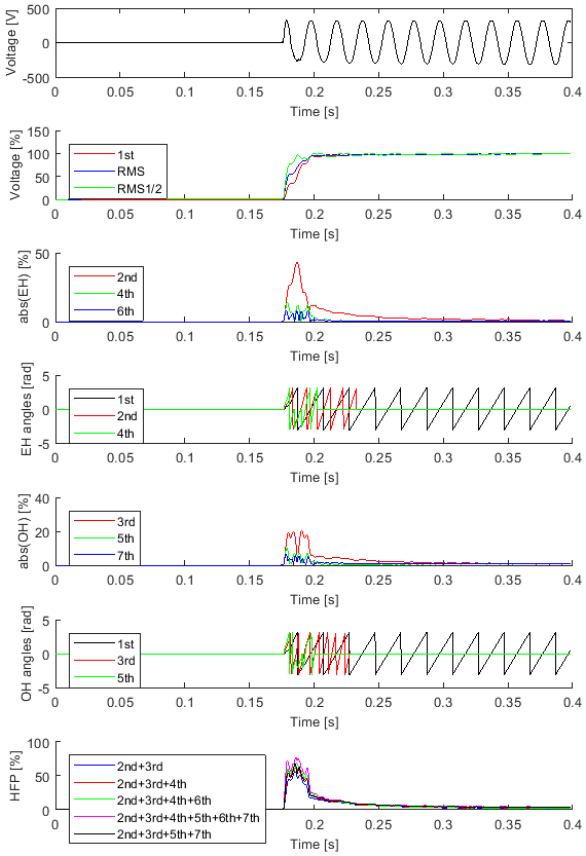

(a)

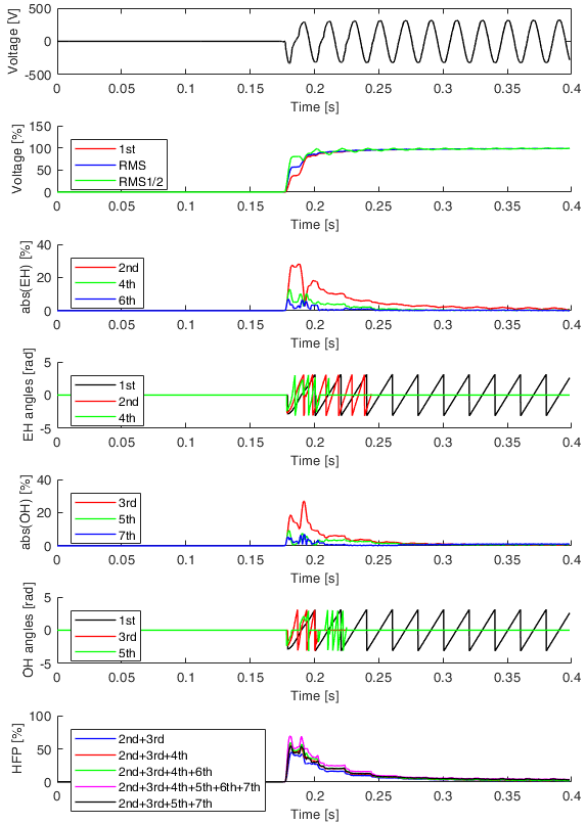

(b)

Fig. 10. The SFFT analysis application on the voltage signals measured during the switching on of the PV power plants

3.3 Correlation between the value of voltage variation and values of voltage harmonics and HFP

This section analyzes the possibility of correlating the magnitude of a voltage variation with the calculated values of HFP. Analyses are done based on the mathematical signals, Eqn. (1), and on the 137 voltage signals detected in real DNs during the voltage dips and swells (including those with a voltage value variation <10%). Different HFPs are analyzed to try to correlate their values with the magnitude of the voltage variation. Since the 2^{nd}, $3^{rd,}$ and 4^{th} harmonics are the most pronounced in Tab. 1, they are used in almost all HFPs, especially the 2^{nd} harmonic. Based on the observations from section 3.2, the following HFPs are considered for mathematical signals: 2^{nd}, $2^{nd}+3^{rd}$, $2^{nd}+3^{rd}+4^{th}$, $2^{nd}+4^{th}+6^{th}$, $2^{nd}+3^{rd}+4^{th}+6^{th}$. The same analysis can be done for any other HFP.

Correlation between the values of HFP with the 10% voltage value variation is done on the mathematical signal defined by Eqn. (1). The voltage phase angle in the moment of the event is varied to estimate its impact on the results. It is observed that for all HFPs calculated results can be best fitted by using a sum of two sine functions, Eqn. (2):

$$L(\phi) = a_1 \cdot \sin\left(b_1 \cdot \varphi + c_1\right) + a_2 \cdot \sin\left(b_2 \cdot \varphi + c_2\right) \qquad (2)$$

where a_1, b_1, c_1, a_2, b_2, and c_2 are empirical coefficients, with their calculated values for different HFPs given in Table 3.

The fitting function for the HFP of $2^{nd}+3^{rd}+4^{th}+6^{th}$ harmonics indicating variation in voltage value equal to 10% for the different phase angle values in the moment of the event is illustrated in Fig. 11.

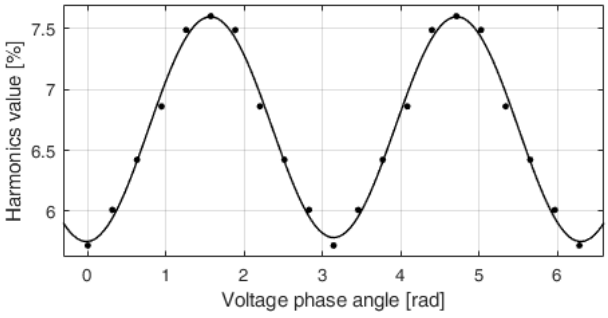

Fig. 11. The fitting function for the HFP of $2^{nd}+3^{rd}+4^{th}+6^{th}$ harmonics indicating variation in voltage value equal to 10% for different phase angle values in the moment of the event

By using Eqn. (2) and values of coefficients from Table 3 it is possible to set the limits for different HFPs and to detect 10% voltage variation of mathematical signals without making any errors.

Table 3. Values of the empirical coefficients a_1, b_1, c_1, a_2, b_2, c_2 in Eqn. (2), which can be used to calculate HFPs limits for a 10% variation of voltage value for different values of phase angle in the moment of the event

HFP	Coefficient						The sum of squares due to error
	a_1 (%)	b_1	c_1 (rad)	a_2 (%)	b_2	c_2 (rad)	
2^{nd}	3.712	0.055	1.397	0.775	1.979	–1.504	0.0178
$2^{nd}+3^{rd}$	5.156	0.103	1.249	0.596	1.875	–1.178	0.3247
$2^{nd}+3^{rd}+4^{th}$	6.116	0.093	1.280	0.777	1.907	–1.279	0.2298
$2^{nd}+4^{th}+6^{th}$	5.743	0.000	1.571	1.699	2.000	–1.572	0.1165
$2^{nd}+3^{rd}+4^{th}+6^{th}$	6.696	0.031	1.473	0.912	1.992	–1.546	0.0876

Table 4. Results of the simplified tests of efficiency of the suggested method for correlation of the voltage value variation and values of HFP

HFP	The max value of (2) indicating variation of voltage value ≥10%	Total number of detected events with a voltage variation <10%	Number of errors
2^{nd}	4.43	72	16 of 72
$2^{nd}+3^{rd}$	5.58		34 of 72
$2^{nd}+3^{rd}+4^{th}$	6.68		35 of 72
$2^{nd}+4^{th}+6^{th}$	7.34		26 of 72
$2^{nd}+3^{rd}+4^{th}+6^{th}$	7.60		36 of 72

The analysis is repeated for the signals measured in real DNs. The results of the tests performed are summarized in Tab. 4. Calculations are performed in a simplified manner: the maximum values of Eqn. (2) indicating a voltage value variation of ≥10% is given in the second column of Tab. 4. Then, 72 cases of detected voltage events with a voltage variation of ≤10% are analyzed, and their HFP is calculated. As can be seen in the fourth column of Tab. 4, this approach was inefficient in many cases since calculations indicate that a voltage variation is >10%, which was incorrect compared to measured data. The cause of these deviations is the harmonic distortion of the grid voltage waveshape in the PCC of PV power plants and of the SH power plant supplying large regulated electric drives, especially during transient events, such as voltage dips and swells. This is discussed in section 3.2, based on the results presented in Tab. 2, Figs. 7b, 7c and 7d.

The calculated values of HFPs for voltage signals measured in the real DNs are presented in Fig. 12. Calculations are done for the following HFPs: 2^{nd}, $2^{nd}+3^{rd}$, $2^{nd}+3^{rd}+4^{th}$, $2^{nd}+4^{th}+6^{th}$, $2^{nd}+3^{rd}+4^{th}+6^{th}$, $2^{nd}+3^{rd}+4^{th}+5^{th}+6^{th}+7^{th}$ and $2^{nd}+3^{rd}+5^{th}+7^{th}$. Figure 12a presents results of calculations for all detected voltage events (137 signals), Fig. 12b presents results only for signals whose voltage variation is ≤20% (113 signals), Fig. 12c presents the same results as Fig. 12b but for limited number of combinations of voltage harmonics to improve graph readability (2^{nd}, $2^{nd}+4^{th}+6^{th}$, $2^{nd}+3^{rd}+5^{th}+7^{th}$), while Fig. 12d presents results only for 2^{nd} harmonic. Very large deviations of calculated results can be noticed, without the possibility of a reliable correlation of the voltage variation value with the values of HFPs. Voltage harmonics in Fig. 12 are calculated relative to the amplitude of the rated phase voltage. Figure 13 presents the same results as Fig. 12b, with the only difference that harmonics are calculated relative to the 1^{st} harmonic. Similar results and conclusions are estimated, as in Fig. 12.

In [11, 22-24] it is reported that HFP can be used for reliable estimation of the voltage dip magnitude and duration. Analyses are mainly conducted on the signals estimated in numerical simulations or on the results measured under laboratory conditions. A limited number of signals from the real DNs were used in tests. In this paper, calculations are done for critical conditions, signals are measured in real DNs, at the PCC of PV power plants, and the SH power plant which supplies large nonlinear loads. The nonlinear characteristics of loads and sources have a significant impact on the characteristics of measured voltage signals, thus making the detection of the voltage value variation by using HFP difficult. That is the reason for the reduced efficiency of the method, estimated in this paper. Further impro-

vement of the method must be made to increase its efficiency in the case of distorted signals measured in real DNs in the presence of nonlinear sources and loads.

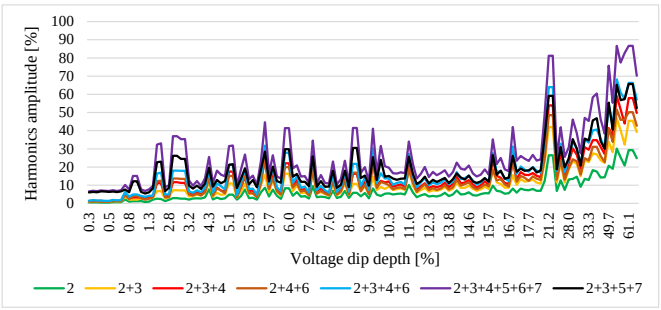

(a)

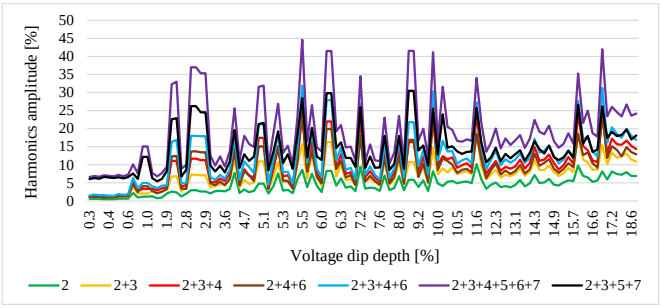

(b)

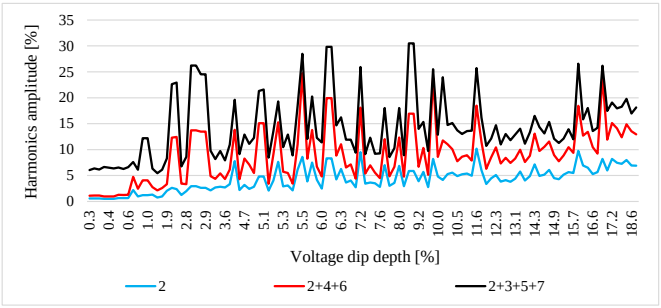

(c)

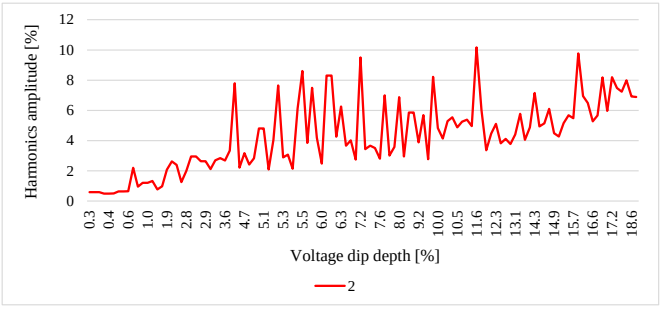

(d)

Fig. 12. Dependence of the HFP values on the voltage value variation for signals measured in real DNs: (a) all detected voltage events (137 signals), (b) only signals with voltage variation ≤20% (113 signals), (c) same as (b) but with a limited number of HFP, (d) same as (b) but for 2nd harmonic

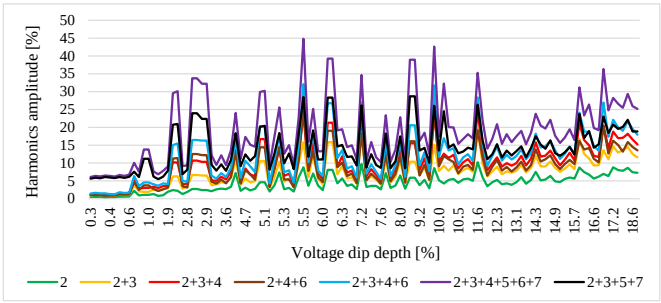

Fig. 13. Dependence of the HFP values calculated relative to the 1st harmonic on the voltage value variation for signals measured in real DNs whose voltage variation is ≤20% (113 signals)

Reliable estimation of the voltage value variation during dips and swells can be done by calculating the voltage RMS value, RMS1/2 value, or value of the 1st voltage harmonic. RMS1/2 voltage value is calculated for the half cycle of the voltage wave (10 ms) and this value converged about two times faster to the steady state value compared to the standard RMS voltage value or value of the 1st voltage harmonic.

4 Conclusion

This paper analyzes the possibility of voltage dips and swells detection based on the SFFT. It is presented that two parameters must be calculated to detect these types of voltage events, amplitudes and phase angles of voltage harmonics. Since the same voltage harmonics values appear in the case of voltage dips and swell, when voltage variation compared to the rated voltage value is the same, by considering phase angles of voltage harmonics it is possible to distinguish these two types of events. It is presented that the phase angles of the higher-order voltage harmonics in the moment of the voltage dip have opposite polarity compared to the phase angle of the 1st harmonic because higher-order harmonics must be subtracted from the 1st harmonic. Also, it is presented that in the case of voltage swells the phase angles of the higher-order harmonics have the same polarity as the phase angle of the 1st harmonic because higher-order harmonics must be added to the 1st harmonic. This conclusion is estimated by analyzing both the mathematical signals and signals measured in the real DNs, in the PCC of renewable energy sources (nine PV power plants and one SH power plant supplying large regulated electric drives). Correlation between the voltage value variation and values of HFPs is done for mathematical signals, considering the dependence on the phase angle of the power frequency voltage at the moment of the event. This correlation is difficult to achieve for signals measured in real DNs because of the impact of nonlinear sources and loads on the voltage waveshape distortion, especially during the transient process. That is the reason for the reduced efficiency of

the method compared to the results from the literature. It is concluded that in the case of distorted signals, SFFT can be used to detect events such as voltage swells and dips, but a more reliable way to estimate the value of voltage variation is to calculate the voltage RMS value, RMS1/2 value (the RMS voltage value calculated for the half cycle of the voltage wave (10 ms)) or the value of the 1st voltage harmonic. All these values are in good agreement, even in the case of strong oscillations of the grid voltage value, mostly during the trip-outs. The fastest way to estimate voltage value variation during the dip or swell is to calculate the RMS1/2 value of the signal. This value converged about two times faster to the steady state value compared to the standard RMS voltage value or the value of the 1st voltage harmonic. In future work, authors will try to correlate some parameters of the HFP with the voltage value variation, to make this method fully applicable in the case of significantly distorted signals measured in modern DNs with nonlinear sources and loads.

References

[1] S. Chattopadhyay, M. Mitra and S. Sengupta, *Electric power quality*, 1st ed., Springer Dordrecht, Berlin/Heidelberg, 2011.

[2] M. Milovanović, J. Radosavljević, B. Perović, J. Vukašinović, A. Jovanović and M. Banjanin, "Point-Estimate Method for Probabilistic Power Flow in Unbalanced and Distorted Distribution Systems," *2024 23rd International Symposium INFOTEH-JAHORINA (INFOTEH)*, East Sarajevo, Bosnia and Herzegovina, pp. 1-6, 2024.

[3] P. Rodríguez-Pajarón, A. Hernández, and J. Milanović, "Probabilistic assessment of the impact of electric vehicles and nonlinear loads on power quality in residential networks", *International Journal of Electrical Power & Energy Systems*, 129:106807, 2021.

[4] L. Alfieri, A. Bracale and A. Larsson, "New power quality indices for the assessment of waveform distortions from 0 to 150 kHz in power systems with renewable generation and modern non-linear loads", *Energies*, vol. 10, no. 10, 1633, 2017.

[5] Voltage characteristics of electricity supplied by public electricity networks, European Standard EN 50160-2010, European Committee for Electrotechnical Standardization (Cenelec), Brussels, 2010.

[6] IEEE recommended practice for monitoring electric power quality, IEEE Std 1159-2009 (Revision of IEEE Std 1159-1995), IEEE, New York, 2009.

[7] IEEE standard for harmonic control in electric power systems, IEEE Std 519-2022 (Revision of IEEE Std 519-2014), IEEE, New York, 2022.

[8] Electromagnetic compatibility (EMC) - Part 4-30: Testing and measurement techniques - Power quality measurement methods, IEC 61000-4-30:2015+AMD1:2021 CSV Consolidated version, International Electrotechnical Commission (IEC), Geneva, 2021.

[9] M. H. J. Bollen, *Understanding power quality problems*, vol. 3. New York: IEEE Press, 2000.

[10] M. Stephens, *Power Quality Standards: CBEMA, ITIC, SEMI F47, IEC 61000-4-11/34*, Electric Power Research Institute, Knoxville, 2009.

[11] V. A. Katić and M. Stanisavljević M, "Smart detection of voltage dips using voltage harmonics footprint", *IEEE Transactions on Industry Applications*, vol. 54, no. 5, pp. 5331-5342, 2018.

[12] M. H. J. Bollen, "Algorithms for characterizing measured three-phase unbalanced voltage dips", *IEEE Transactions on Power Delivery*, vol 18, no. 3, pp. 937-944, 2003.

[13] M. R. Alam, K. M. Muttaqi and A. Bouzerdoum, "Characterizing voltage sags and swells using three-phase voltage ellipse parameters", *IEEE Transactions on Industry Applications*, vol. 51, no. 4, pp. 2780-2790, 2015.

[14] M. Barghi Latran and A. Teke, "A novel wavelet transform based voltage sag/swell detection algorithm", *International Journal of Electrical Power & Energy Systems*, vol. 71, pp. 131-139, 2015.

[15] J. R. Barros, I. Diego, and M. de Apráiz, "Applications of wavelets in electric power quality: voltage events", *Electric Power Systems Research*, vol. 88, pp. 130-136, 2012.

[16] W. X. Hu, X. Y. Xiao, and Z. X. Zheng, "Voltage sag/swell waveform analysis method based on multi-dimension characterisation", *IET Generation, Transmission & Distribution*, vol. 14, no. 3, pp. 486-493, 2020.

[17] E. A. Nagata, D. D. Ferreira, C. A. Duque, and A. S. Cequeira, "Voltage sag and swell detection and segmentation based on Independent Component Analysis", *Electric Power Systems Research*, vol. 155, pp. 274-280, 2018.

[18] R. Cisneros-Magaña, A. Medina and O. Anaya-Lara, "Time-domain voltage sag state estimation based on the unscented Kalman filter for power systems with nonlinear components", *Energies*, vol. 11, no. 6, 1411, 2018.

[19] Z. Li, R. Yang, X. Guo, Z. Wang, and G. Chen, "A novel voltage sag detection method based on a Selective Harmonic Extraction algorithm for nonideal grid conditions", *Energies*, vol. 15, no. 15, 5560, 2022.

[20] Z. Wang, X. Guo, Z. Li, H. Lin, and G. Chen, "A fast voltage sag detection method based on second order generalized integrator and delay transform method", *Energy Reports*, vol. 8, no. 13, pp. 549-556, 2022.

[21] G. T. Heydt, P. S. Fjeld, C. C. Liu, D. Pierce, L. Tu and G. Hensley, "Applications of the windowed FFT to electric power quality assessment", *IEEE Transactions on Power Delivery*, vol. 14, no. 4, pp. 1411-1416, 1999.

[22] V. A. Katić and A. M. Stanisavljević, "Novel voltage dip detection algorithm using harmonics in the dip's transient stage", *In: IECON 2017 - The 43rd Annual Conference of the IEEE Industrial Electronics Society*, pp. 351-356, Beijing, China, October 29 - November 01, 2017.

[23] A. M. Stanisavljević, V. A. Katić, and S. L. Milićević, "A method for real-time prediction of the probability of voltage sag duration based on harmonic footprint", *IEEE Access*, Vol. 10, pp. 23757-23773, 2022.

[24] A. M. Stanisavljević, and V. A. Katić, "Magnitude of Voltage Sags Prediction Based on the Harmonic Footprint for Application in DG Control System", *IEEE Transactions on Industrial Electronics*, vol. 66, no. 11, pp. 8902-8912, Nov. 2019.

[25] https://www.metrel.si/en/shop/PQA/mi-2892.html

[26] The MathWorks Inc. (2023). MATLAB version: 9.13.0 (R2023b), Natick, Massachusetts: The MathWorks Inc. https://www.mathworks.com

Received 14 November 2024